ORIGINAL PAPER

# Impact of Main Boundary Thrust (MBT) on Landslide Susceptibility in Garhwal Himalaya: A Case Study

Ritu Raj Nath[1] · Nani Das[2] · D. Neelima Satyam[3]

**Abstract** In Garhwal Himalayan region, seismicity plays a major role in inducing mass movement. Especially at places where active faulting occurs, multiple and retrogressive slope failures have been observed. The active tectonism of the Himalayan collision zone makes the whole mountain chain fragile and instable. In this context, an endeavor has been made in the present study to correlate the impact of Main Boundary Thrust (MBT) on the overall landslide susceptibility for a 74-km stretch of NH 7 in the Garhwal Himalaya, using statistical models of landslide susceptibility zonation (LSZ) mapping. The results of the study show that slope angle, road network and distance from MBT are the most crucial landslide causative parameters in the study area, with statistical contribution of 26%, 20% and 18%, respectively. The study also produces an accurate LSZ map for this stretch of NH 7, which shows that almost 30% of the area has high to very high degree of landslide susceptibility. The prepared LSZ map will be of practical significance for institutionalizing any future landslide mitigation programs in the study area.

✉ Ritu Raj Nath
rituraj nath14@gmail.com

[1] Department of Civil Engineering, Assam down town University, Sankar Madhab Path, Panikhaiti, Guwahati, Assam 781029, India

[2] Department of Earth Sciences, IIT Roorkee, Roorkee 247667, India

[3] Department of Civil Engineering, IIT Indore, Indore 453331, India

## Introduction

Landslides are one of the most destructive natural phenomena, which seem ubiquitous throughout the Himalayan mountain chains. Several instances of catastrophic landslides in the Himalaya were reported by various researchers [1–4] in the past three decades. Himalayan landslides are often fatal, and it is estimated that over 1000 people were killed in landslide events in the Himalaya, which represents almost 35% of the global total [1, 5]. Also, the economic losses associated with landslide hazards are substantial in this region, which is approximately projected at INR 1000–1500 million per year [6]. The rugged topography, complex geological structures, fragile soil cover, high-intensity monsoon rainfall and the occurrence of very large magnitude earthquake events are crucial causative parameters of landslides in the Himalaya [1, 7]. The frequency of landslide in the Himalaya is further intensified due to the occurrence of a wide range of material contrast in the whole region, along with the uneven spatial distribution of sheared materials, jointed and fissured materials, adversely oriented discontinuities and permeability contrasts [1]. Especially at plate terrain boundaries, where different lithologies are juxtaposed, frequent and large-scale slope failures have been observed, which may be ascribed to the continuous uplift and rebound caused by the hyperactive Himalayan seismicity [7]. Shorder argued that in the Himalaya, seismicity has been a major factor in inducing mass movement [7]. Particularly, at places where active faulting occurs, retrogressive and multiple slope failures are observed in the same locality [1]. In this context, Garhwal Himalaya presents a very interesting case study, where landslide swarms are observed in the vicinity of active Main Boundary Thrust (MBT) [8, 9]. Main Boundary Thrust (MBT) is one of the major structural

features of the Himalayan belt that forms the present-day structural and orographic boundary between the Outer and Lesser Himalayas [10]. As generally is the case with neo-tectonically active areas, the incidences of landslide events are extensive in the Garhwal Himalayan region [8], which is believed to be an exceptional segment of the Himalayan collision zone [11].

As the general consensus, it is accepted that major tectonic features play an important role in landslide occurrence [12–16] and thus are considered as an important contributory factor while assessing the landslide susceptibility of a particular region [1, 17, 18]. Keefer [12] used fault rupture zone as one of the five parameters to relate landslide distribution with earthquake activities for 40 historical worldwide earthquake databases and observed that for great earthquake with magnitudes greater than 8, landslide activities can be traced as far as 200 km from fault rupture zones. Similar observations were recorded by Rodrıguez et al. [13] with a bigger dataset of 76 historical earthquakes. Liao and Lee [14] documented 9272 large landslides induced by Chi-Chi earthquake in 1999 ($M_L$ = 7.3) and observed that the greatest distance between the landslide and the fault rupture plane ranged from 60 to 70 km. Xu et al. [16] considered the distance from fault as a major geologic controlling factors of landslides for carrying out the Yushu earthquake-triggered landslide hazard mapping in China. Bhattacharya et al. [19] noticed slow surface movements of the Mansa Devi landslide relative to neighboring area during 1992–1998 and concluded that the present landslide is a cumulative effect of those slow surface movements. The study concluded that apart from the earthquakes generated due to the slip in an active fault, the aseismic fault motions also control the rate and occurrence of landslides near major tectonic features [19]. Pachauri and Pant [20] observed a positive relationship between the Aglar fault and landslide activities of the area, where maximum landslide distribution was reported in the proximity of the fault [20].

These studies demonstrated that in assessing the overall landslide susceptibility of a region, it is important to consider the effect of fault distance comprehensively. However, for the Himalayan region, only few studies [21–23] have indicated the positive correlation between the fault distance and landslide incidences. There is a general paucity of studies quantifying the effect of fault distance on landslide incidences for the Himalayan belt in general, and especially for the Garhwal zone. In this context, an endeavor has been made in the present study to statistically correlate the possible impact of MBT on landslide susceptibility for a part of Garhwal Himalaya. An updated and accurate landslide susceptibility zonation (LSZ) map is also produced for the study area using statistical method.

## Study Area

This study has been carried out for approximately 74-km stretch of Nation Highway NH-7, starting from Rishikesh and up to Devprayag, in the Uttarakhand state of India. The study area exhibits the complex and still evolving geology of the Garhwal Himalaya [24]. The Himalayan orogeny consists of five tectonic assemblages that are juxtaposed along the Tertiary faults of the Himalayan thrust belt [25]. It is bounded by a frontal thrust zone in the south and the Indus–Tsangpo suture zone in the north [26]. The Himalaya has been geologically divided into four litho-tectonic subdivisions [27] from south to north: (a) Outer Himalaya that mostly includes the molassic Siwalik Supergroup of Mio-Pliocene ages and is demarcated by two tectonic plates, the Main Frontal Thrust (MFT) to the south and the Main Boundary Thrust (MBT) to the north; (b) Lesser Himalaya that exposes a thick pile of highly folded Proterozoic sedimentary strata together with a few outcrops of older crystalline rocks; this subdivision is bounded by the Main Boundary Thrust (MBT) to the south and the Main Central Thrust (MCT) to the north; (c) Greater or Higher Himalaya that exposes a massive, north-dipping pile of metamorphic rocks—the central crystalline zone—and is demarcated by the MCT to its south and the Dar-Martoli Fault or Tethys Fault or the South Tibetan Detachment (STD) to the north; and (d) Tethys Himalaya that includes with a thick pile of sedimentary rocks of Cambrian to Lower Eocene ages. The present study area falls in the Lesser Himalayan sub-division. The Main Boundary Thrust (MBT) is the regional thrust passed through to the study area [28]. Valdiya [23] reported to have observed the shreds of evidence for neo-tectonism and reactivation of faults and thrust throughout the NW Himalaya that includes the study area. A map of the study area is presented in Fig. 1a. The identified geological formations [23, 24, 29, 30] in the study area are: Lower Siwalik group, Jaunsar group of Western Himalaya, Krol, Infrakrol and Blaini formation, Tal formation of Western Himalaya and Subathu formation. The most commonly available rock types are: sandstone, mudstone, limestone, shales, dolomitic gray limestone, conglomerate, etc. A geological map of the study area is shown in Fig. 1b.

The study area is characterized by very rugged terrain, extensively bounded by peaks of variable heights and several valleys. The main river that traverses throughout the study area is the Ganga, which is formed by the confluence of two rivers, viz. Alakananda and Bhagirathi at Devprayag. The study area receives average annual rainfall of approximately 1229 mm. The peak season for the monsoon in this region is from June to September, which contributes about 50–90% of the annual rainfall budget.
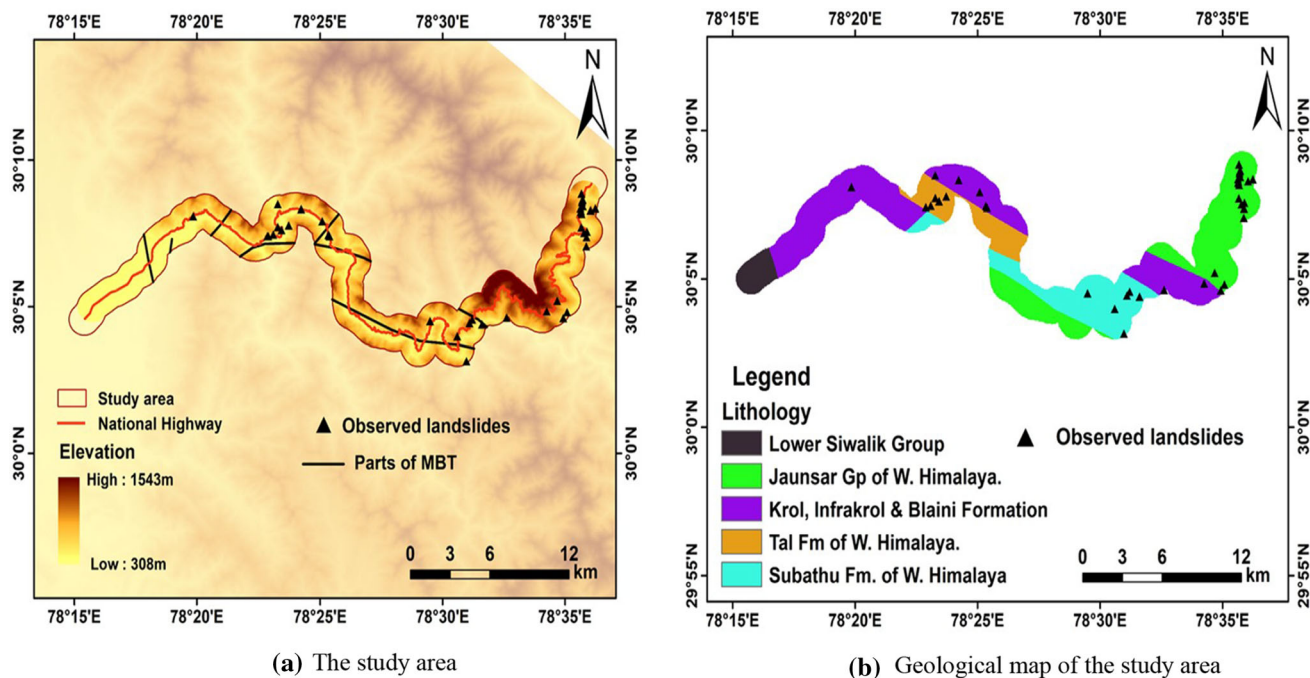
**(a)** The study area



**(b)** Geological map of the study area

**Fig. 1 a** The study area. **b** Geological map of the study area

During summer, day temperature increased to about 45 °C, and during winter, the temperature falls below 5 °C [31, 32].

## Methodology

The study envisages to statistically correlate the fault effect on landslide susceptibility, and therefore, it is imperative to use a statistical model of landslide susceptibility zonation (LSZ) mapping. In this context, landslide relative frequency (LRF) method [33–37] provides with an excellent platform, where it is possible to quantify the statistical contribution of the individual landslide causative factors. The methodology adopted in this study incorporates the following steps:

1. Preparation of a landslide distribution map for the study area.
2. Identification of the existing landslide causative parameters in the study area and creation of a database for the same using various sources.
3. Rasterization and creation of thematic layers for landslide causative parameters.
4. Performance of spatial analyses.
5. Performance of statistical analyses to quantify the role of MBT in landslide susceptibility.

LRF method is a modification of frequency ratio (FR) method [33, 34], where the FRs are normalized in the range

of probability values [0, 1] as relative frequency [38]. Mathematically, FR and LRF can be expressed as

$$FR_i = \frac{N_i / \sum N_i}{A_i / \sum A_i} \qquad (1)$$

where $FR_i$ = frequency ratio of the $i$th class of a thematic layer of a landslide causative factor; $N_i$ = number of observed landslides in the $i$th class of a thematic layer; $\sum N_i$ = total number of observed landslides in that thematic layer; $A_i$ = of the $i$th class of a thematic layer; $\sum A_i$ = total area of that thematic layer.

$$LRF = \frac{Factor\ Class\ FR}{\sum Factor\ Class\ FR}. \qquad (2)$$

After the normalization, the LRFs have still the disadvantage of considering all causative factors as equal weight. To solve this problem and to consider the mutual interrelationship among the independent variables, predictor rating ($R_i$) is calculated as given in Eq. (3):

$$R_i = \frac{(LRF_{max} - LRF_{min})_i}{(LRF_{max} - LRF_{min})_{min}}. \qquad (3)$$

Generally, value of $R_i$ is normalized to indicate the statistical contribution of a particular parameter in landslide susceptibility. $R_i$ and LRF are numerically integrated in a GIS environment to produce the LSZ map of the study area. A schematic diagram of the working methodology is presented in Fig. 2, which is self-explanatory.
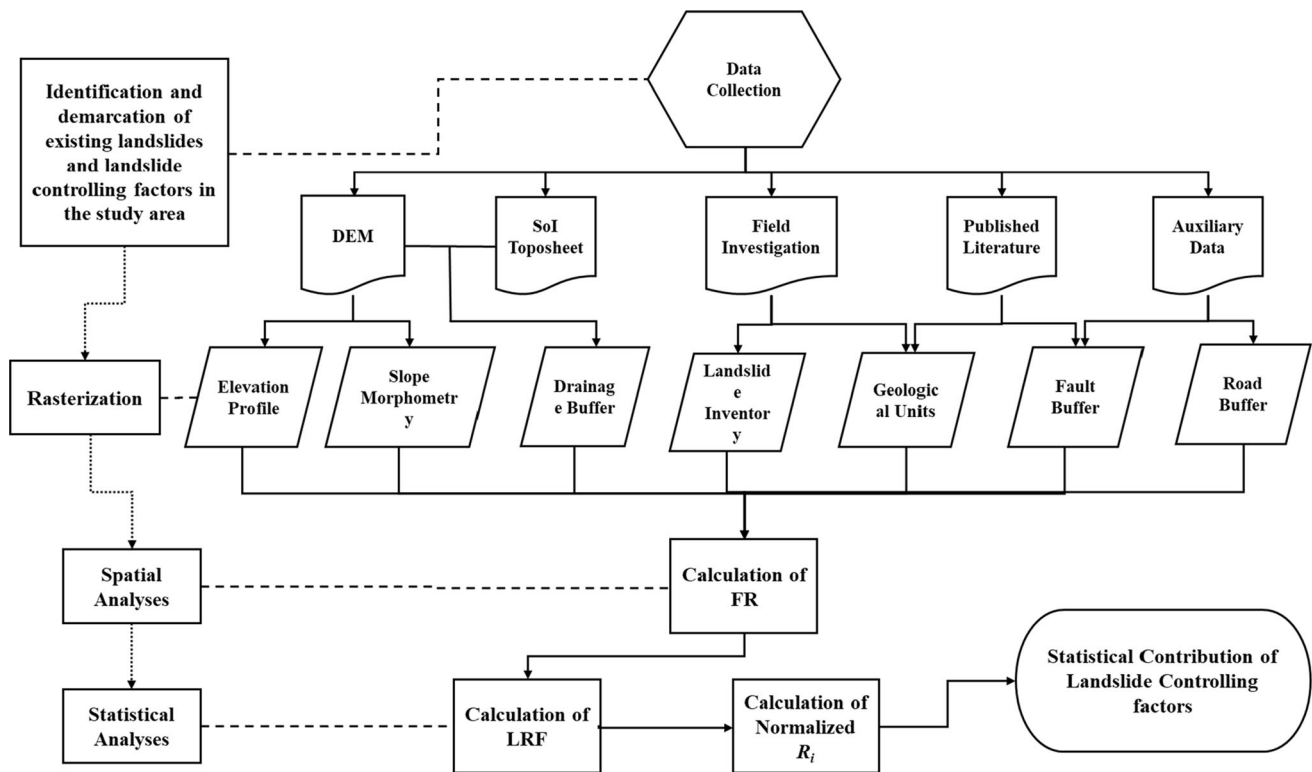
**Fig. 2** Schematic diagram of the working methodology

## Preparation of Landslide Distribution Map

Identification and mapping of the existing landslides in an area is the first and most important task for landslide hazard analysis. In this study, a total of 38 numbers of landslides are identified through field survey (Fig. 3a, b), which are then mapped in a GIS environment (Fig. 1a) to prepare the landslide distribution map. The prepared landslide distribution map is further used as a thematic layer for proximity analysis.

It is observed that out of 38 landslides, 17 slides show circular failure pattern and 14 slides show planer mode of failure. Five numbers of wedge and two numbers of block failures are also observed in the study area. This indicates that circular failure is the predominant mode that constitutes around 45% of total slides, followed by planer failure mode which represents almost 37%. The corresponding figures for wedge and block failures are 13% and 5%.

## Identification of Landslide Causative Parameters in the Study Area

Four major categories of landslide causative parameters are identified for the Himalayan belt, which are geological, morphological, physical and anthropogenic [1, 7]. Based on these categories, seven landslide causative parameters are considered for the study area. Table 1 presents a

detailed discussion on the landslide causative parameters of the study. They are further classified as internal/preparatory or external/triggering class [1, 17].

It is to be noted that different researchers have considered several other landslide causative factors for LSZ studies in the Himalaya [1, 8, 17]. However, for the study area the seven landslide causative parameters are identified through detailed field investigations and published literature. These seven causative factors are considered extensively for almost all the LSZ studies carried out for the Himalayan region. A detailed discussion on the geology of the study area is presented in Sect. 2. The geological map (Fig. 1b) is used as a thematic layer for the study.

## Preparation of Thematic Layers

### Digital Elevation Model [DEM] and Its Derivatives

The surface topography of an area can be derived in the form of digital elevation model (DEM). DEM represents the spatial variation of elevation of an area digitally. Data for elevation, slope angle, slope aspect and drainage density buffer for the study area have been extracted from *ASTER GDEM V.2.0* [39] with 30 m resolution. The elevation profile of the study area ranges from 308 to 1543 m above MSL (mean sea level). The DEM of the study area is

**(a)** A typical observed landslide in the

study area (*30° 08.015′, 78° 35.565′*)



**(b)** A typical observed landslide in the

study area (*30° 06.543′, 78° 35.016′*)

**Fig. 3** **a** A typical observed landslide in the study area (30° 08.015′, 78° 35.565′). **b** A typical observed landslide in the study area (30° 06.543′, 78° 35.016′)

**Table 1** Landslide causative parameters for the study area

| S. no. | Landslide causative parameter | Category | Class | Remarks |
|---|---|---|---|---|
| 1 | Lithology/geological units | Geological | Internal/ preparatory | There exists a wide range of material contrast in the whole Himalayan region. The uneven spatial distribution of sheared materials, jointed and fissured materials, adversely oriented discontinuities and permeability contrasts make the Himalaya very susceptible to landslide hazard |
| 2 | Slope angle | Morphological | Internal/ preparatory | The slope angles in this region range between 30° and 70° leading to the formation of near vertical slip surfaces |
| 3 | Slope aspect | Morphological | Internal/ preparatory | Aspects of the slope implicate a local effect and are generally considered on region-specific basis |
| 4 | Elevation | Morphological | Internal/ preparatory | The Himalaya is the tallest mountain in the world, and therefore, the available relief through which slope failure can act is the greatest |
| 5 | Distance from major tectonic features | Physical | Internal/ preparatory | The effect of uplift and rebound, especially at plate terrene boundaries, where different lithologies are juxtaposed, can be reasoned with the repetitive slope failures in the Himalaya |
| 6 | Distance from drainage | Physical | Internal/ preparatory | The high rate and volume of discharge throughout the Himalaya, especially high-velocity downstream flow, cause a great deal of fluvial erosion in the mountains |
| 7 | Distance from road | Anthropogenic | External/ triggering | A rapid rise in infrastructures including roads, hydropower stations and dams, etc., with inadequate or little consideration for the natural hazards has considerably contributed to triggering of landslides in the Himalaya |

shown in Fig. 1a. It is further categorized into five classes (Fig. 4a).

The DEM is used to derive various terrain attributes such as slope angle (Fig. 4b), slope aspect (Fig. 4c) and the drainage density of the study area, which are used as input data layers for LSZ mapping. The drainage density map is further validated using Survey of India (SoI) toposheets [40] at a scale of 1:50,000. From the drainage density map, drainage Euclidean distance map (Fig. 4d) is prepared in the GIS environment. In this study, the thematic layers are

**Fig. 4** **a** Elevation map of the study area. **b** Slope angle map of the study area. **c** Slope aspect map of the study area. **d** Drainage Euclidean distance map of the study area. **e** Fault Euclidean distance map of the study area. **f** Road Euclidean distance map of the study area



(a) Elevation map of the study area

(b) Slope Angle map of the study area

(c) Slope Aspect map of the study area

(d) Drainage Euclidean distance map of the study area

(e) Fault Euclidean distance map of the study area

(f) Road Euclidean distance map of the study area
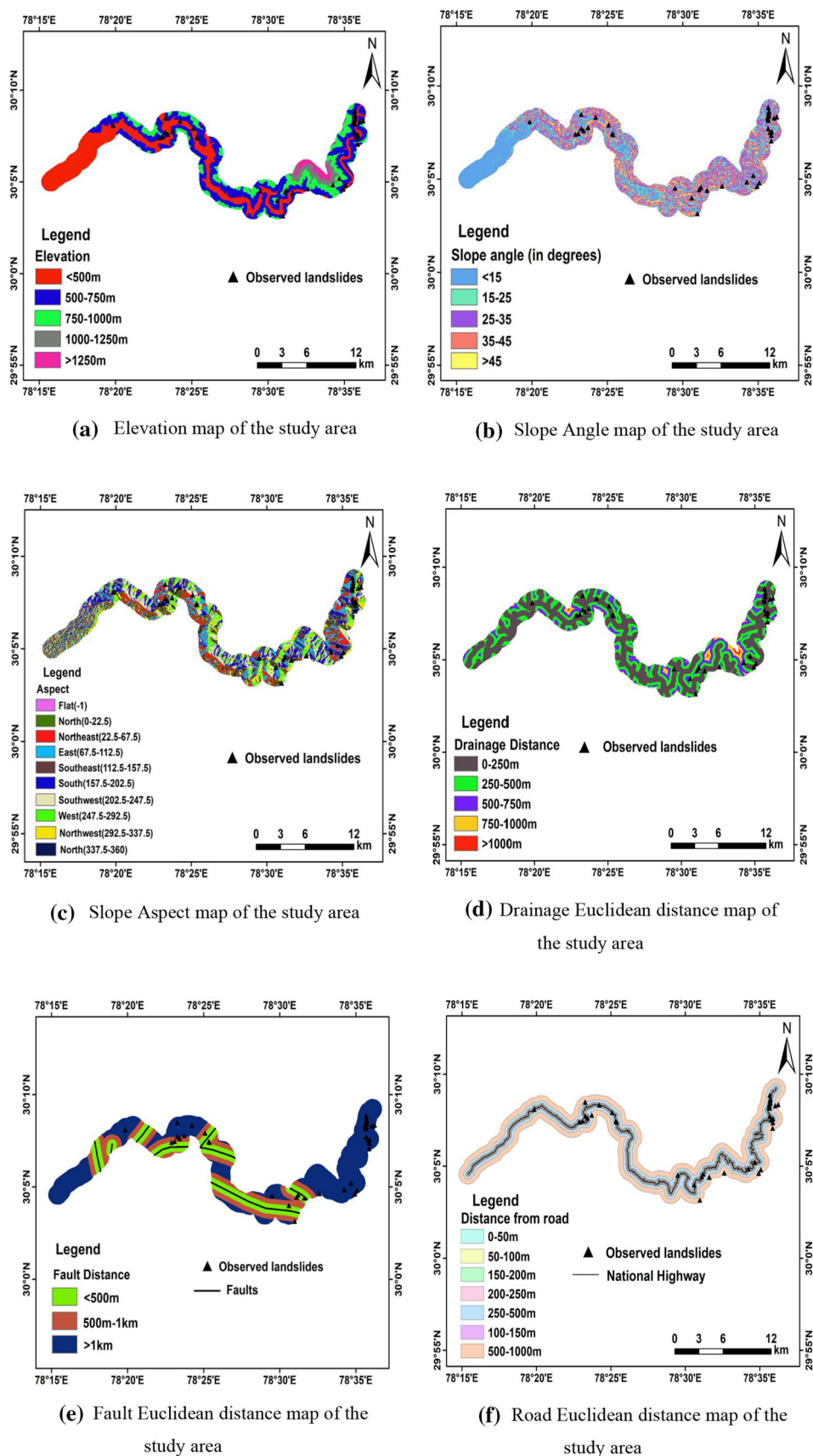
prepared for a 1-km buffer zone on each side of the NH-7 [old NH-58]. Following the conventional methods of LSZ mapping, each of these thematic layers is further categorized into five classes for spatial analyses.

## Fault Euclidean Distance Map

Main Boundary Thrust (MBT) is the major fault, traversing throughout the study area. The fault contour map of the study area is prepared using the seismotectonic atlas of India [41]. The digitized fault contours are exported in the GIS environment to calculate the Euclidean distance of the existing landslides from the nearest source (fault). The fault Euclidean distance map of the study area is shown in Fig. 4e. It is categorized into five classes.

## Road Euclidean Distance Map

A 74-km stretch of NH 7 throughout the study area has been digitized, and a 1-km buffer zone is created on its both sides in the GIS environment. The road buffer is then used to calculate the Euclidean distance of the existing landslides. It is further categorized into seven classes (Fig. 4f).

## Results and Discussion

The prepared thematic layers are collated and analyzed both spatially and statistically to calculate the FRs and LRFs for each factor class using Eqs. (1) and (2). The results are shown in Table 2.

The LRFs are used to calculate the predictor rating ($R_i$) for each landslide causative parameter to evaluate their statistical contribution toward the overall landslide susceptibility of the study area. The results are shown in Table 3.

The results show that slope angle is the most crucial landslide causative factor in the study area, with a statistical contribution of around 26% toward the overall landslide susceptibility. Particularly, the slopes with inclination greater than 25° are much susceptible to landslides. Due to ingress of roads in the fragile mountain chains of the Himalaya, the number of landslide incidences increases manifold. Since 2014, road widening projects have been implemented continuously on NH 7, and its negative impact is rather discernable in the study area. Statistically, distance from road contributes approximately 20% to landslide susceptibility. With a $R_i$ value of 0.18, distance from MBT is found out to be the third most significant parameter of landslide susceptibility in the study area. In fact, the relative importance of fault distance is calculated to be greater than that of elevation profile and drainage

distance, which is indeed a very interesting observation. One thing should be noted that near homogeneity of slope forming materials leads to assigning a smaller, nonsignificant $R_i$ value to lithological units. It may be interpreted as landslides have occurred almost uniformly on all types of lithological units, and thus, the effect is nullified. The same explanation may be given to the smaller $R_i$ value of slope aspect parameter.

To better augment the finding of the research work, an LSZ map of the study area has been prepared. For that purpose, the calculated predictor rating for each thematic layer and relative frequencies of each factor class are numerically integrated in a GIS environment to calculate landslide susceptibility index (LSI) [36–38] for each pixel. The LSI values are then reclassified using natural breaks into five classes to produce the final LSZ map of the study area (Fig. 5). The prepared LSZ map shows five distinct zones of landslide susceptibility: Very Low (VLS), Low (LS), Moderate (MS), High (HS) and Very High (VHS). Further analyses of the LSZ map reveal that although only $\sim 10$ km$^2$ area falls in the VHS zone, it contains 18 out of 38 observed landslides. Similarly, 14 numbers of landslides are observed in HS zone that constitutes $\sim 27$ km$^2$ of the study area, and 5 landslides are observed in the MS zone. VLS and LS zones contain 0 and 1 observed landslide, respectively. Overall, around 40% of the total study area is observed to have very low to low landslide susceptibility, approximately 30% of the study area shows moderate landslide susceptibility, and the remaining 30% falls under high to very high landslide susceptibility. The resultant analysis of the prepared LSZ map is given in Table 4.

It is observed from Table 4 that although the zone of very high landslide susceptibility constitutes the lowest percentage of the total area ($\sim 8$%), it contains the highest concentration of observed landslide ($\sim 48$%). On the other hand, the lowest percentage of landslides is observed for the low and very low susceptibility zone ($\sim 3$%). The landslide density per square km for the very high susceptible zone is 2.021, which is distinctly larger than for the other susceptible zones. Also, there is a gradual decrease in frequency of observed landslide per square km from the very high to the very low susceptible zones with considerable separation. Hence, it can be concluded that the classified susceptibility zones are in good agreement with occurrences of preexisting landslides. It is further confirmed by the frequency ratio (FR) analysis of landslide susceptibility zones that compares the similarity between susceptibility zones and landslide inventory (Fig. 6a). Analysis of the success rate curve [42] is used in this study to qualitatively assess the accuracy of the predictive map. The success rate curve is obtained by plotting the cumulative percentage of observed landslide occurrence against

**Table 2** Calculation of frequency ratio and landslide relative frequency for various classes of thematic layers

| Factor class | No. of observed landslides ($N_i$) in the class | Area of the factor class ($A_i$) (km$^2$) | FR | LRF |
|---|---|---|---|---|
| *Geological units* | | | | |
| Lower Siwalik Group | 0 | 5.15 | 0 | 0 |
| Jaunsar group of Western Himalaya | 19 | 33.26 | 1.77507 | 0.39588 |
| Krol, Infrakrol and Blaini formation | 8 | 45.53 | 0.54591 | 0.12175 |
| Tal formation of Western Himalaya | 5 | 11.65 | 1.33378 | 0.29746 |
| Subathu formation | 6 | 22.49 | 0.82909 | 0.18490 |
| *Elevation* | | | | |
| < 500 m | 6 | 41.76 | 0.44640 | 0.07693 |
| 500–750 m | 19 | 53.65 | 1.10032 | 0.18962 |
| 750–1000 m | 8 | 14.59 | 1.70409 | 0.29367 |
| 1000–1250 m | 5 | 6.09 | 2.55201 | 0.43979 |
| > 1250 m | 0 | 1.98 | 0 | 0 |
| *Slope angle* | | | | |
| < 15° | 0 | 28.15 | 0.26232 | 0.02267 |
| 15°–25° | 2 | 21.43 | 0.32279 | 0.02790 |
| 25°–35° | 4 | 34.84 | 1.26310 | 0.10916 |
| 35°–45° | 12 | 26.71 | 9.72238 | 0.84027 |
| > 45° | 24 | 6.94 | 0.26232 | 0.02267 |
| *Slope aspect* | | | | |
| Flat | 0 | 0.40 | 0 | 0 |
| N | 1 | 14.45 | 0.61921 | 0.08058 |
| NW | 3 | 15.05 | 2.32057 | 0.30197 |
| E | 12 | 16.06 | 1.31552 | 0.17118 |
| SE | 7 | 16.53 | 1.01602 | 0.13221 |
| S | 6 | 18.34 | 1.00216 | 0.13041 |
| SW | 5 | 15.50 | 0.26372 | 0.03432 |
| W | 1 | 11.78 | 0.93278 | 0.12138 |
| NW | 3 | 9.80 | 0.21488 | 0.02796 |
| *Drainage Euclidean distance* | | | | |
| 0–250 m | 20 | 61.15 | 1.01631 | 0.37462 |
| 250–500 m | 16 | 38.83 | 1.28021 | 0.47189 |
| 500–750 m | 2 | 14.92 | 0.41640 | 0.15349 |
| 750–1000 m | 0 | 2.85 | 0 | 0 |
| > 1000 m | 0 | 0.32 | 0 | 0 |
| *Fault Euclidean distance* | | | | |
| < 500 m | 6 | 33.47 | 0.55695 | 0.19205 |
| 500–1000 m | 5 | 42.12 | 0.36901 | 0.12724 |
| > 1000 m | 27 | 42.50 | 1.97410 | 0.68071 |
| *Road Euclidean distance* | | | | |
| < 50 m | 19 | 7.07 | 8.35422 | 0.65153 |
| 50–100 m | 6 | 6.92 | 2.69599 | 0.21026 |
| 100–150 m | 2 | 6.48 | 0.95963 | 0.07484 |
| 150–200 m | 0 | 6.35 | 0 | 0 |
| 200–250 m | 0 | 6.30 | 0 | 0 |
| 250–500 m | 4 | 29.63 | 0.41946 | 0.03271 |
| 500–1000 m | 7 | 55.33 | 0.39310 | 0.03066 |

**Table 3** Calculation of normalized $R_i$ for landslide causative parameters

| Parameter | $LRF_{Max}$ | $LRF_{Min}$ | $LRF_{Max}$–$LRF_{Min}$ | $R_i$ | Normalized $R_i$ |
|---|---|---|---|---|---|
| Slope angle | 0.840 | 0.023 | 0.818 | 5.709 | 0.26 |
| Road | 0.652 | 0.031 | 0.621 | 4.335 | 0.20 |
| Fault | 0.681 | 0.127 | 0.553 | 3.864 | 0.18 |
| Elevation | 0.439 | 0.076 | 0.363 | 2.531 | 0.12 |
| Drain | 0.472 | 0.153 | 0.318 | 2.223 | 0.10 |
| Lithology | 0.396 | 0.122 | 0.274 | 1.914 | 0.09 |
| Slope aspect | 0.171 | 0.028 | 0.143 | 1.000 | 0.05 |
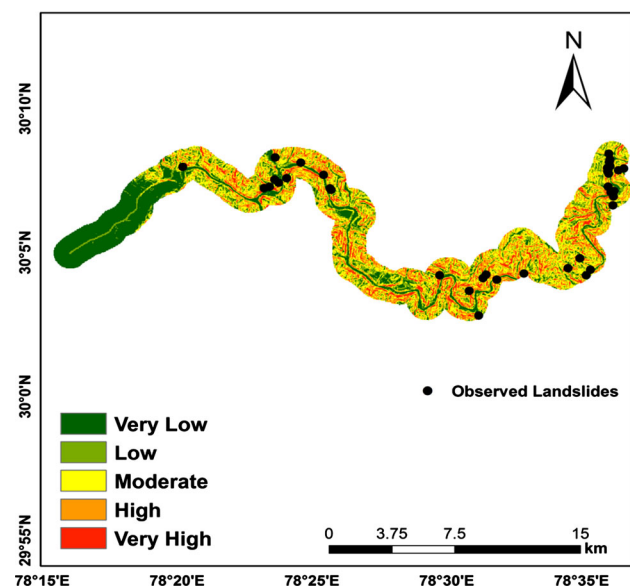


**Fig. 5** The landslide susceptibility zonation (LSZ) map of the study area

the cumulative percentage of LSZ area (Fig. 6b). Area under the success rate curve is 0.8315, indicating an overall success of the prepared LSZ map as ∼ 83.15%, which is in accord with the acceptable norm used for the Himalayan LSZ studies [18].

The prepared LSZ map has been validated both statistically and physically (through field survey), and it shows a

reasonable scenario of the current susceptibility level for the study area. This confirms that not only the prepared LSZ map is practically satisfactory, but the findings of the study in terms of statistical contribution of the various landslide causative parameters for the study area could also be physically acceptable. Thus, it can be argued that the presence of MBT has indeed increased the overall landslide susceptibility of the study area.

## Conclusion

In this study, an endeavor has been made to statistically correlate the impact of MBT on landslide susceptibility for a part of Garhwal Himalaya using statistical model of LSZ mapping. It is observed that for this area, the contribution of MBT on overall landslide susceptibility is a significant 18%. Similarly, statistical contributions of other landslide causative parameters are assessed, and it is observed that slope morphometry and the proximity to the existing road are two other significant landslide causative parameters. Particularly, landslides induced by anthropogenic factor (such as road network widening projects, construction of dam) become an area of major concern. This implies that necessary mitigation measures must be initiated by the government, as the ongoing road widening projects of NH 7 seem to render additional instability to the already fragile mountain chains of the Himalaya. The results of the study

**Table 4** Analysis of the LSZ map of the study area

| Landslide susceptibility zone | Area (km²) | Ratio of the zone area to the total area | No. of observed landslides | % of observed landslides in the zone | Observed landslides frequency per km² |
|---|---|---|---|---|---|
| Very low | 26.52 | 0.22 | 0 | 0 | 0 |
| Low | 21.37 | 0.18 | 1 | 2.6 | 0.047 |
| Moderate | 33.98 | 0.30 | 5 | 13.2 | 0.147 |
| High | 27.30 | 0.22 | 14 | 36.8 | 0.513 |
| Very high | 8.91 | 0.08 | 18 | 47.4 | 2.021 |

**(a)** *FR* analysis of LSZ map
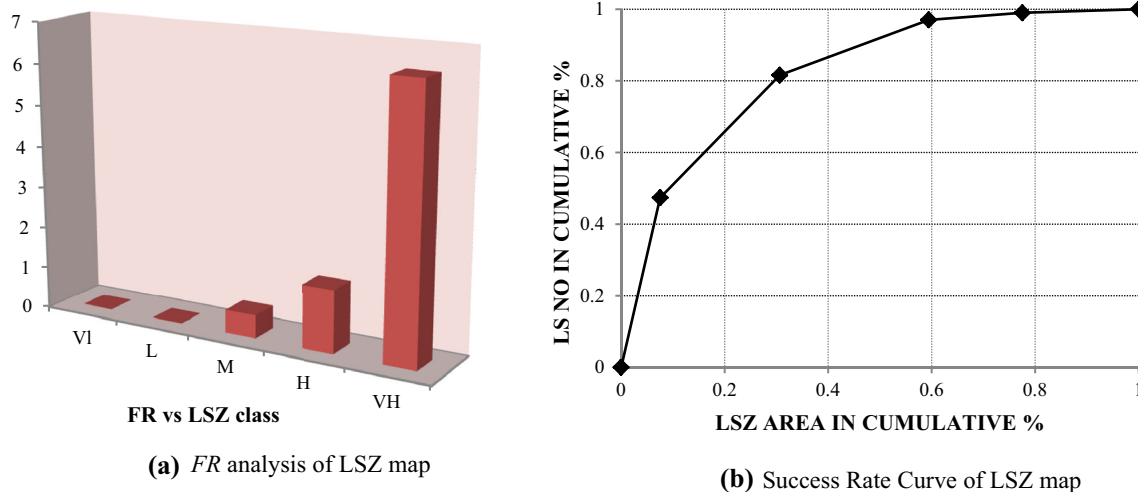


**(b)** Success Rate Curve of LSZ map

**Fig. 6** *FR* analysis of LSZ map. **b** Success Rate Curve of LSZ map

show an idiosyncratic impact of MBT on overall landslide susceptibility of the study area. For this study area, the relative importance of MBT as an internal landslide causative parameter is significantly greater than that of either elevation or drainage distance. In classical approach of LSZ mapping, the prevalent consensus is that relative relief and drainage distance might have a bigger impact on landslide susceptibility. However, when we consider Himalayan landslides, this doctrine needs re-examination, considering the hyper-active tectonism of the Himalaya. The present research work has shown statistically that for the study area, impact of MBT on landslide susceptibility is far greater than commonly recognized, and thus requires further investigations to be able to understand its full implications.

## References

1. Nath RR, Sharma ML, Tyagi A (2020) Review of the current practice on inclusion of seismicity in landslide susceptibility zonation: a case study for Garhwal Himalaya. Himalayan Geol 41(2):222–233
2. Rautela P, Pande RK (2005) Traditional inputs in disaster management: the case of Amparav, North India. Int J Environ Stud https://doi.org/10.1080/00207230500034586
3. Nadim F, Kjekstad O, Peduzzi P et al (2006) Global landslide and avalanche hotspots. Landslides. https://doi.org/10.1007/s10346-006-0036-1
4. Dortch JM, Owen LA, Haneberg WC et al (2009) Nature and timing of large landslides in the Himalaya and Transhimalaya of northern India. Quat Sci Rev. https://doi.org/10.1016/j.quascirev.2008.05.002
5. Petley D (2012) Global patterns of loss of life from landslides. Geology. https://doi.org/10.1130/G33217.1
6. National Landslide Risk Management Strategy. A publication of the National Disaster Management Authority, Government of India. September 2019, New Delhi
7. Shroder JF (1998) Slope failure and denudation in the western Himalaya. Geomorphology. https://doi.org/10.1016/S0169-555X(98)00052-X
8. Sarkar S, Kanungo DP, Mehrotra GS (1995) Landslide hazard zonation: a case study in Garhwal Himalaya. Mt Res Dev, India. https://doi.org/10.2307/3673806
9. Pachauri AK, Gupta PV, Chander R (1998) Landslide zoning in a part of the Garhwal Himalayas. Environ Geol. https://doi.org/10.1007/s002540050348
10. Mugnier JL, Huyghe P, Chalaron E, Mascle G (1994) Recent movements along the Main Boundary Thrust of the Himalayas: normal faulting in an over-critical thrust wedge? Tectonophysics. https://doi.org/10.1016/0040-1951(94)90056-6
11. Khattri KN, Chander R, Gaur VK et al (1989) New seismological results on the tectonics of the Garhwal Himalaya. Proc Indian Acad Sci Earth Planet Sci. https://doi.org/10.1007/BF02880378
12. Keefer DK (1984) Landslides caused by earthquakes. Bull Geol Soc Am. https://doi.org/10.1130/0016-7606(1984)95%3c406:lcbe%3e2.0.co;2
13. Rodríguez CE, Bommer JJ, Chandler RJ (1999) Earthquake-induced landslides: 1980–1997. Soil Dyn Earthq Eng. https://doi.org/10.1016/S0267-7261(99)00012-3
14. Liao HW, Lee CT (2000) Landslides triggered by the Chi-Chi earthquake. In: Proceeding of the 21st Asian conference on remote sensing, vol 1(2), pp 383–388
15. Chigira M, Yagi H (2006) Geological and geomorphological characteristics of landslides triggered by the 2004 Mid Niigta prefecture earthquake in Japan. Eng Geol. https://doi.org/10.1016/j.enggeo.2005.10.006
16. Xu C, Xu X, Lee YH et al (2012) The 2010 Yushu earthquake triggered landslide hazard mapping using GIS and weight of evidence modeling. Environ Earth Sci. https://doi.org/10.1007/s12665-012-1624-0
17. Kanungo DP, Arora MK, Sarkar S, Gupta RP (2009) Landslide susceptibility zonation (LSZ) mapping—a review. J South Asia Disaster Stud. http://hdl.handle.net/123456789/786
18. Kayastha P, Dhital MR, De Smedt F (2013) Application of the analytical hierarchy process (AHP) for landslide susceptibility mapping: A case study from the Tinau watershed, West Nepal. Comput Geosci. https://doi.org/10.1016/j.cageo.2012.11.003
19. Bhattacharya A, Mukherjee K, Kuri M, et al (2015) Potential of SAR intensity tracking technique to estimate displacement rate in

a landslide-prone area in Haridwar region, India. Nat Hazards. https://doi.org/10.1007/s11069-015-1949-6

20. Pachauri AK, Pant M (1992) Landslide hazard mapping based on geological attributes. Eng Geol. https://doi.org/10.1016/0013-7952(92)90020-Y

21. Kothyari GC, Pant PD, Luirei K (2012) Landslides and neotectonic activities in the Main Boundary Thrust (MBT) zone: Southeastern Kumaun, Uttarakhand. J Geol Soc India. https://doi.org/10.1007/s12594-012-0123-y

22. Pant PD, Luirei K (1999) Malpa rockfalls of 18 August 1998 in the northeastern Kumaun Himalaya. J Geol Soc India 54(4):415–420

23. Valdiya KS (2003) Reactivation of Himalayan frontal fault: implications. Curr Sci 85(7):1031–1040

24. Valdiya KS (1984) Evolution of the Himalaya. Tectonophysics. https://doi.org/10.1016/0040-1951(84)90205-1

25. Gehrels GE, DeCelles PG, Martin A et al (2003) Initiation of the Himalayan orogen as an early Paleozoic thin-skinned thrust belt. GSA Today. https://doi.org/10.1130/1052-5173(2003)13%3c4:IOTHOA%3e2.0.CO;2

26. Yin A (2006) Cenozoic tectonic evolution of the Himalayan orogen as constrained by along-strike variation of structural geometry, exhumation history, and foreland sedimentation. Earth-Sci Rev. https://doi.org/10.1016/j.earscirev.2005.05.004

27. Aitchison JC, Ali JR, Davis AM (2007) When and where did India and Asia collide? J Geophys Res Solid Earth. https://doi.org/10.1029/2006JB004706

28. Siddique T, Pradhan SP, Das N, et al (2020) Stabilization of Cut Slopes along the Highway by Optimizing Geometry, NH-58, Lesser Himalaya. J Geol Soc India. https://doi.org/10.1007/s12594-020-1507-z

29. Najman Y, Garzanti E (2000) Reconstructing early Himalayan tectonic evolution and paleogeography from Tertiary foreland basin sedimentary rocks, northern India. Bull Geol Soc Am. https://doi.org/10.1130/0016-7606(2000)112%3c435:REHTEA%3e2.0.CO;2

30. Ray L, Bhattacharya A, Roy S (2007) Thermal conductivity of Higher Himalayan Crystallines from Garhwal Himalaya, India. Tectonophysics. https://doi.org/10.1016/j.tecto.2007.02.003

31. Indian Meteorological Department, Ministry of Earth Sciences, Government of India, https://mausam.imd.gov.in. Accessed on 20/09/2020

32. Khandelwal DD, Gupta AK, Chauhan V (2015) Observations of rainfall in Garhwal Himalaya, India during 2008–2013 and its correlation with TRMM data. Curr Sci. https://doi.org/10.18520/cs/v108/i6/1146-1151

33. Lee S, Pradhan B (2007) Landslide hazard mapping at Selangor, Malaysia using frequency ratio and logistic regression models. Landslides. https://doi.org/10.1007/s10346-006-0047-y

34. Mohammady M, Pourghasemi HR, Pradhan B (2012) Landslide susceptibility mapping at Golestan Province, Iran: A comparison between frequency ratio, Dempster-Shafer, and weights-of-evidence models. J Asian Earth Sci. https://doi.org/10.1016/j.jseaes.2012.10.005

35. Ozdemir A, Altural T (2013) A comparative study of frequency ratio, weights of evidence and logistic regression methods for landslide susceptibility mapping: Sultan mountains, SW Turkey. J Asian Earth Sci. https://doi.org/10.1016/j.jseaes.2012.12.014

36. Kumar R, Anbalagan R (2015) Landslide susceptibility zonation in part of Tehri reservoir region using frequency ratio, fuzzy logic and GIS. J Earth Syst Sci. https://doi.org/10.1007/s12040-015-0536-2

37. Sangeeta, Maheshwari BK (2019) Earthquake-Induced Landslide Hazard Assessment of Chamoli District, Uttarakhand Using Relative Frequency Ratio Method. Indian Geotech J. https://doi.org/10.1007/s40098-018-0334-2

38. Acharya TD, Lee DH (2019) Landslide susceptibility mapping using relative frequency and predictor rate along Araniko Highway. KSCE J Civ Eng 23(2):763–776

39. NASA/METI/AIST/Japan Spacesystems, and U.S./Japan ASTER Science Team. ASTER Global Digital Elevation Model V002. 2011, distributed by NASA EOSDIS Land Processes DAAC

40. Survey of India, Department of Science and Technology, Government of India. Available online: http://www.surveyofindia.gov.in/. Accessed on 2nd April, 2018

41. Dasgupta S et al (2000) Seismotectonic Atlas of India and its Environs. Geol Surv India Spec Publ

42. Chung CJF, Fabbri AG (1999) Probabilistic prediction models for landslide hazard mapping. Photogramm Eng Remote Sens 65(12):1389–1399